The electronic spectroscopy and structure of complexes of argon with 3aminos tetrazine in a supersonic jet

Joseph C. Alfano, Selso J. Martinez III, and Donald H. Levy

Citation: The Journal of Chemical Physics **94**, 1673 (1991); doi: 10.1063/1.459939
View online: http://dx.doi.org/10.1063/1.459939
View Table of Contents: http://scitation.aip.org/content/aip/journal/jcp/94/3?ver=pdfcov
Published by the AIP Publishing

The electronic spectroscopy and structure of complexes of argon with 3-amino-*s*-tetrazine in a supersonic jet

Joseph C. Alfano, Selso J. Martinez III, and Donald H. Levy
The James Franck Institute and the Department of Chemistry, The University of Chicago, Chicago, Illinois 60637

(Received 27 August 1990; accepted 22 October 1990)

The structure and spectroscopy of van der Waals clusters between argon and 3-amino-*s*-tetrazine (AT) has been investigated in a supersonic jet. Low resolution vibrationally resolved fluorescence excitation spectra of AT at a variety of argon gas concentrations enable us to assign the origin transitions for the clusters AT–Ar_n, where $n = 1$ through 6. The frequencies of the van der Waals vibrational modes of these clusters are determined, both in the excited states from the excitation spectra, and in the ground state from single vibronic level emission spectra. High resolution spectroscopy is used to resolve rotational structure in the origin transitions of some of the clusters, and this provides structural information about the clusters. The argon atom in AT-Ar is found to be above the tetrazine ring, and the argon atoms in AT–Ar_2 are found to be above and below the tetrazine ring, in all cases having a van der Waals bond length of about 3.3 Å. This work is useful in interpreting the results of our previous study on the photodissociation dynamics of van der Waals clusters between argon and AT.

I. INTRODUCTION

Since the earliest uses of supersonic jets in spectroscopy, van der Waals clusters have been an area of intense study. One class of van der Waals clusters which has been a subject of much investigation is complexes involving an argon atom bound to a single ring aromatic molecule. Systems studied include tetrazine–Ar[1-6] (T–Ar), benzene–Ar,[7] aniline–Ar[8], dimethyltetrazine–Ar[9] (DMT–Ar), pyrimidine–Ar[10], *p*-difluorobenzene–Ar,[11-12] and styrene–Ar.[13] Recently, Knight *et al.*[14] have obtained mass-selected resonant enhanced multiphoton ionization spectra of aniline–Ar, phenol–Ar, fluorobenzene–Ar, and chlorobenzene–Ar, using an elegant delayed ion extraction technique which surpresses spectral contributions from dissociating complexes. The dissociation dynamics of some of these systems have been investigated. Additionally, in some cases rotational analysis of vibronic transitions has been performed to extract structural and geometric information.[15] In most cases the cluster has the argon atom centered over the aromatic ring at its van der Waals radius. In the aniline–Ar complex, however, Yamanouchi *et al.*[8] raise the intriguing possibility that the argon atom may not be located directly above the center of the aromatic ring, but instead may be displaced toward the amino group.

Recently we extended these studies by examining the dissociation dynamics of the complexes between 3-amino-*s*-tetrazine (AT) and argon[16] (see Fig. 1). We found striking examples of mode selectivity in the photodissociation process, where the dissociation rate of AT–Ar varies by a factor of 200 depending on which of several closely lying ring vibrational modes is excited. Additionally, we studied the photophysics of AT–Ar_2 dissociation, and found the branching ratio of the two possible photoproducts (AT and AT–Ar) to vary with the initially excited mode. The cause of this extreme mode selectivity is currently not well understood, especially since similar clusters such as T–Ar[2,4,6] and DMT–Ar[17] show very little mode selective behavior.

Here we have undertaken an investigation into the structure and basic spectroscopy of various clusters between argon and AT. Our motivation is twofold. First, this information will shed light on our previous dynamical studies, and hopefully give us insight into the puzzling behavior of AT–Ar clusters. The difference in the dissociation behavior between AT–Ar and T–Ar may reflect differences in their cluster geometries, or also may reflect differences in the van der Waals density of states caused by different frequencies of their van der Waals modes. This study will address both of these points. Secondly, the geometry of complexes between argon and AT raises interesting structural questions. In previous high resolution rotationally resolved studies of clusters of this type, with the exception of aniline–Ar, the argon atom was always located over the center of the aromatic ring. In aniline–Ar, the symmetry of the aniline subunit does not

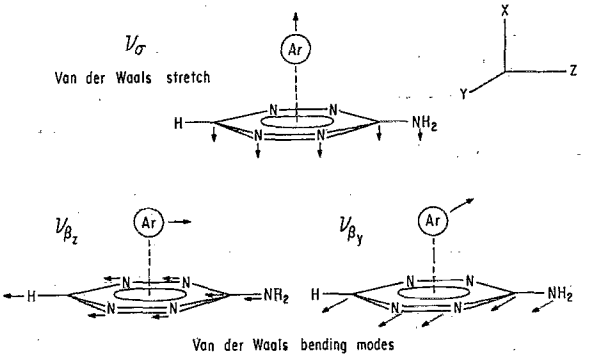

FIG. 1. The aminotetrazine–argon cluster (AT–Ar), and the three van der Waals vibrational modes. The coordinate system used in the paper, which is based on the Mulliken convention, is also shown.

 0021-9606/91/031673-11$03.00

preclude structures in which the argon atom is not directly over the center of the ring. Yamanouchi *et al.*[8] performed a band contour analysis of the aniline–Ar origin rotational contour and proposed a geometry in which the argon atom is displaced from the ring center toward the amino group by 0.6 ± 0.5 Å. The large error bars, caused by the moderate resolution of the experiment ($0.04\ cm^{-1}$), preclude a definitive determination if the argon atom is indeed displaced from the ring center. Likewise, in AT–Ar, the argon atom is not restricted by the symmetry of the AT subunit to be centered over the ring. The amino group is a strong perturbation on the tetrazine ring, as the amino lone pair participates in the aromatic π system, and the C–NH_2 bond has a partial double bond character. Perhaps in AT the amino group distorts the charge density of the ring sufficiently to displace the argon binding site from the center of the ring towards the amino group. Thus, in a qualitative way we can view the position of the argon atom as a sensitive probe of the AT electronic structure which can give us insight into the charge distribution of the tetrazine ring. The 100 MHz ($0.003\ cm^{-1}$) resolution of our experiment is over an order of magnitude higher than in the previous aniline–Ar study,[8] and thus we hope to be able to determine the geometry of the AT–Ar complex to sufficiently high precision to determine if the argon is displaced from the ring center.

We start by looking at low resolution vibrationally resolved fluorescence excitation spectra. Argon concentration studies enable us to identify the origin transition of various argon clusters, and we use this to assign van der Waals vibrational frequencies in the excited state. Single vibronic level (SVL) emission spectra enable us to obtain van der Waals vibrational frequencies in the ground electronic state. Finally, we use high resolution spectroscopy to rotationally resolve the origin transition for several argon clusters, which gives us structural information for these clusters.

II. EXPERIMENTAL

The experimental apparatus has been described in detail previously,[18–20] and hence only a brief description will be given here. The aminotetrazine-seeded supersonic jet was generated by passing helium over a reservoir of AT heated in an oven to 80 °C, then expanding the mixture through a 100 μ pinhole. Argon was seeded into the expansion using a Unit mass flow controller (model UFC-1200A). Laser induced fluorescence spectra were generated by crossing the supersonic jet with the output of an argon ion pumped dye laser operating with either Rhodamine 110 or Coumarin 535. For total fluorescence scans the fluorescence was imaged with a camera lens onto a slit, which served to limit laser scattering and reduce Doppler broadening by transmitting fluorescence only from the cold core of the jet. The fluorescence passing through the slit was detected by a cooled photomultiplier tube (RCA C31000A) in a photon counting configuration. The fluorescence as a function of laser frequency was normalized for fluctuations in laser power and digitally recorded. For dispersed fluorescence scans, the fluorescence was imaged onto the entrance slits of 1 m monochromator. The dispersed fluorescence signal was normalized using the simultaneously collected total fluorescence signal.

Two types of total fluorescence scans were taken: low resolution and high resolution. For low resolution scans, we used an argon ion pumped home-built standing wave dye laser with a birefringent filter as the only tuning element. This enabled us to scan hundreds of cm^{-1} with a resolution of about 1 cm^{-1}. For high resolution scans, a Coherent 699-29 ring dye laser was used instead of the standing wave laser. This ring laser has a nominal linewidth of 0.5 MHz; Doppler broadening limited our experimental resolution to about 90 MHz.

AT was synthesized according to the literature by Dr. D. D. Yang.[21,22]

III. LOW RESOLUTION VIBRATIONALLY RESOLVED FLUORESCENCE EXCITATION SPECTRA

A. Argon concentration studies

Figures 2(a) through 2(d) show low resolution fluorescence excitation spectra in the region of the AT monomer origin transition for a variety of argon concentrations. As can be seen in Fig. 2(b), upon bleeding in even a small amount of argon, features begin to grow in to the red of the AT monomer origin. These features are clearly due to the formation of clusters between AT and argon atoms. At higher argon concentrations, the spectra become extremely congested and complicated.

Initially, we used these concentration studies to tentatively determine the nature of the argon cluster transitions. In general, the intensity of a transition of a cluster of AT with n argon atoms (AT–Ar_n) will increase relative to the intensity of the monomer as the concentration of argon raised to the nth power, provided cluster formation is a kinetically controlled process. The feature at 18 383 cm^{-1} increases approximately linearly with argon concentration relative to the monomer origin, and is hence assigned as the origin transition of the AT–Ar complex. Similarly, the transition at 18 355 cm^{-1} scales quadratically with argon concentration relative to the origin of the AT monomer, and is thus assigned as the AT–Ar_2 origin. Transitions further to the red increase even faster with argon concentration, and are clearly due to higher argon oligimers. It becomes difficult to extract quantitatively the argon concentration dependence of these higher oligimers owing to spectral congestion; nonetheless, we tentatively make the assignments shown in Fig. 2(d) and tabulated in Table I. These assignments are supported by band shift information described in the next section, and conclusively confirmed by high resolution rotationally resolved spectra discussed in Sec. V.

B. Argon cluster band shifts

The shift of argon cluster transitions from the corresponding transition of the monomer frequently provides information regarding the identity and, in favorable cases, the structure of the argon clusters. The AT–Ar origin is red shifted 27 cm^{-1} with respect to the AT monomer; this is very close to the band shift of T–Ar[15] and DMT–Ar[9]. This suggests that AT–Ar has a geometry similar to that of these other complexes, in which the argon atom is centered above

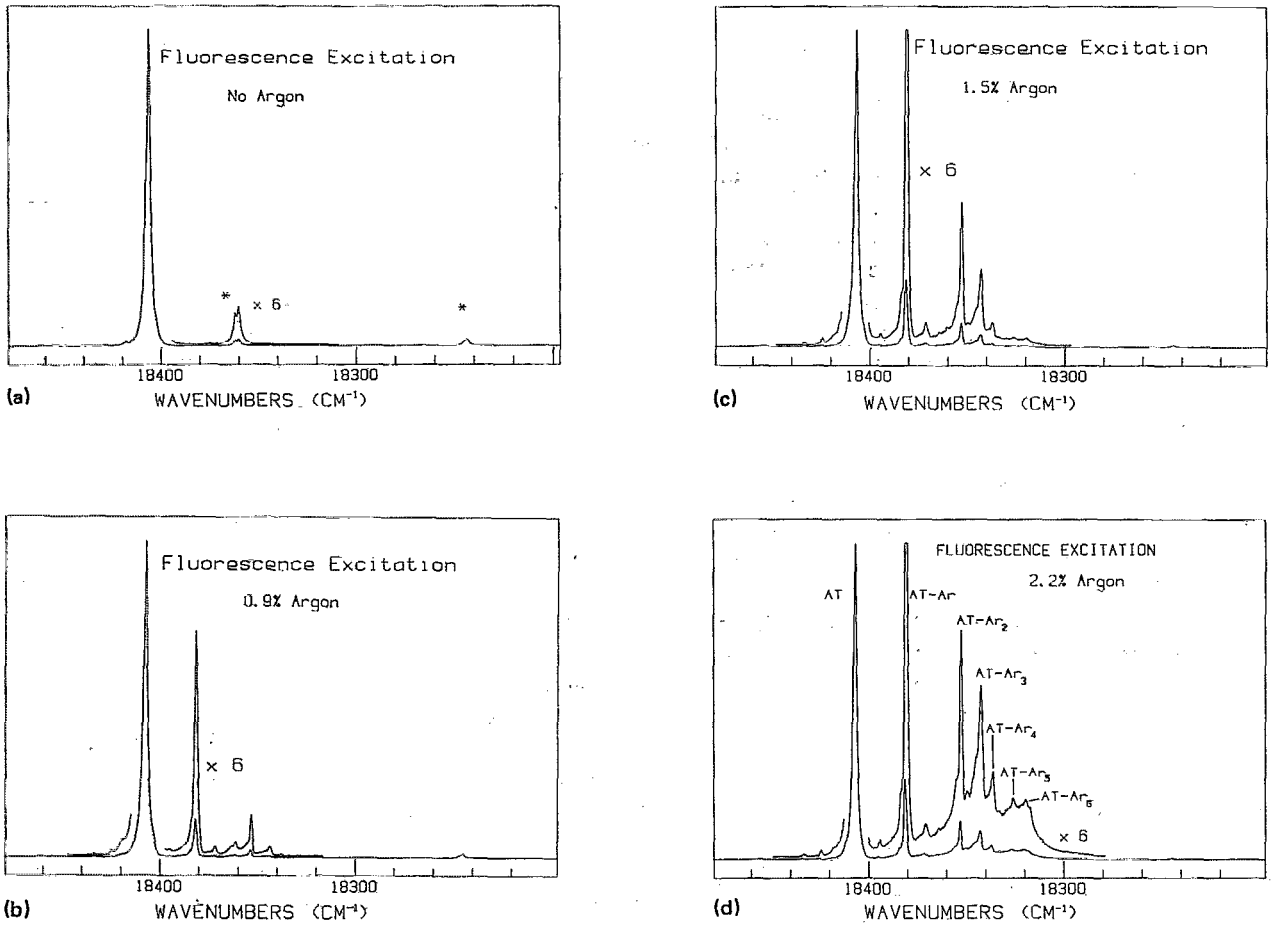

FIG. 2. Low resolution fluorescence excitation spectra taken near the origin region of the AT monomer, as a function of argon concentration. The spectra were taken using a 100 μ pinhole with 2.7 atm of total pressure. (a) No added argon. The feature marked with stars are the I_1^1 monomer inversion hot band and a second unassigned hot band, respectively. (b) 0.9% argon, (c) 1.5% argon, (d) 2.2% argon. The labels mark the origin transitions of the various argon cluster species.

TABLE I. Features and assignments in the fluorescence excitation spectrum of AT seeded with 2.2% argon.

ν(cm^{-1})[a]	Intensity[b]	Species	Transition
18 438	0.002	AT–Ar_2	σ_0^2
18 428	0.004	AT–Ar	σ_0^1
18 422	0.006		
18 410	1.000	AT	0_0^0
18 398	0.010	AT–Ar_2	σ_0^1
18 384	0.256	AT–Ar	0_0^0
18 375	0.010	AT–Ar_2 isomer[c]	0_0^0
18 355	0.121	AT–Ar_2	0_0^0
18 346	0.093	AT–Ar_3	0_0^0
18 340	0.047	AT–Ar_4	0_0^0
18 330	0.033	AT–Ar_5	0_0^0
18 324	0.032	AT–Ar_6	0_0^0

[a] Typical uncertainty is $\pm$ 1 cm^{-1}.
[b] Intensity is relative to the AT monomer origin, which is normalized to 1.000.
[c] The feature at 18 375 cm^{-1} is assigned to the origin transition of an isomer of AT–Ar_2 in which both argon atoms are on the same side of the ring, as described in the text.

the tetrazine ring, at a distance of about 3.4 Å.[15] The origin of AT–Ar_2 is located 55 cm^{-1} to the red of the AT monomer origin. This band shift is twice the band shift of the AT–Ar complex, within the resolution of our experiment. According to the band shift rule,[23] this indicates that both argon atoms occupy equivalent binding sites. The incremental band shift of clusters of AT with three and four argon atoms is 9 and 5 cm^{-1}, respectively. These shifts are much smaller that the 27 cm^{-1} band shift observed for the first two complexes between AT and argon, which indicates that the third and fourth argon atoms bind to sites which are not equivalent to the sites occupied by the first and second argon atoms. In T–Ar_3, rotationally resolved spectroscopy showed the third argon to lie above an argon already bound to the ring, which may be similar to the structure for AT–Ar_3. The band shift of the fourth argon atom is about half that of the third argon atom; this may be because the binding site of the fourth argon is not equivalent to that of the third argon, or as is more likely, may indicate that complications such as many body effects are causing a breakdown of the band shift rule.

We assign the peaks shifted -81 and $-89\ cm^{-1}$ from the monomer origin as the origin transitions of AT–Ar_5 and AT–Ar_6. The features in this region are extremely broad and dense, most likely due to many different isomers and higher argon oligimers.

In addition to the origin transition, argon cluster bands are seen to the red of all higher AT vibrational levels. The cluster band shifts for different levels of AT are shown in Table II. In almost all cases, the cluster band shifts of these higher vibrational levels mirror the behavior of the origin level. The one vibrational level which shows anomalous behavior is the $16b^2$ level, which has band shifts of -10 and $-22\ cm^{-1}$ for the one and two argon complex, respectively. This differs from T–Ar, in which it is the $16a^2$ level which shows anomalous behavior. Weber and Rice have shown that band shifts for a given vibrational level are related to the first and second derivative of the van der Waals potential with respect to the normal coordinate for the given vibrational mode.[6] The differences in the band shifts of the $16a^2$ and $16b^2$ levels in T–Ar and AT–Ar, respectively, suggest that the intermolecular van der Waals potential of these two species differ along the $16a$ and $16b$ normal modes.

C. van der Waals vibrational modes

In addition to the origin transition of the various argon clusters assigned above, there are other weak features which owing to their argon concentration dependence can be attributed to low-frequency cluster vibrations. Each argon atom in the cluster adds three additional vibrational degrees of freedom to the complex; these additional degrees of freedom are known as the van der Waals vibrational modes. Normal mode analysis done by Bernstein *et al.*[24] show that for clusters between simple aromatics and single rare gas atoms, such as T–Ar and benzene–Ar, the three additional normal modes are the van der Waals stretch (υ_σ) and two orthogonal van der Waals bending modes ($\upsilon_{\beta y}$ and $\upsilon_{\beta z}$), shown in Fig. 1. Note that the coordinate system in Fig. 1, which is based on the Mulliken convention, is different from that used by Berstein and others.[14,24,25] For an aromatic molecule bound to two argon atoms, one on each side of the ring, there are six van der Waals vibrational modes, presumably one symmetric stretch, one antisymmetric stretch, and four bending modes. For higher polymers, speculation regarding the van der Waals normal modes becomes problematic, and must await a normal mode analysis.

Knight *et al.*[14] have demonstrated that in substituted benzene–argon clusters there is extensive mixing between the van der Waals bending and stretching modes in the region of the van der Waals stretching fundamental. This Fermi resonance causes the normal modes shown in Fig. 1 to merely be basis functions onto which the true vibrational eigenfunctions can be expanded. This mixing has a significant effect on the intensity and, to a lesser extent the position of the van der Waals transitions seen in their mass-selected resonant enhanced multiphoton ionization spectra. They have determined the off-diagonal coupling matrix elements to range between 0.5 and 4.5 cm^{-1}, thus the shift of the vibrational eigenvalues relative to the zeroth order energies is on the order of a few cm^{-1}. As it is difficult to perform resonant enhanced multiphoton ionization spectroscopy on AT–Ar_n complexes since the ionization energy is much greater than the energy of two resonant photons, we cannot mass select our spectra. Thus we do not attempt the analysis done by Knight *et al.*,[14] and instead assign our spectra in terms of zeroth order normal modes shown in Fig. 1, while pointing out that owing to anharmonic coupling these normal modes may only be approximations to the true vibrational eigenfunctions. We base our van der Waals frequency assignments on the argon concentration studies, as well as previous assignments made on tetrazine–rare gas clusters.[25]

TABLE II. Band shifts of argon cluster species relative to the corresponding AT monomer transition.

	Number of argons in complex					
Level	1	2	3	4	5	6
0_0^0	27[a]	55	64	69	81	89
$16b_0^2$	10	22	...[b]	...	...	...
$16a_0^2$	26	55	...	...	...	...
$6a_0^1$	26	54	64	69	80	86
1_0^1	27	54	65	72	...	...
$6a_0^2$	26	54	65	72	...	...
$6a_0^1 1_0^1$	25	53	...	...	...	...

[a] The accuracy of our measurements is estimated to be $\pm 1\ cm^{-1}$.
[b] Dots indicate that the corresponding transition is too weak to be observable.

1. AT–Ar symmetric stretch

There is a small peak at 18 428 cm^{-1}, partially overlapping with the monomer origin, whose intensity increases with argon concentration at the same rate as does the AT–Ar origin transition. Thus it is clearly attributable to a low frequency $+44\ cm^{-1}$ vibration of the AT–Ar complex. The wavenumber of the van der Waals symmetric stretch of T–Ar is 44 cm^{-1}, identical to the wave number of this low frequency AT–Ar vibration. We thus assign the feature at 18 428 cm^{-1} to the AT–Ar symmetric stretch fundamental σ_0^1, whose normal mode is shown in Fig. 1. As in T–Ar, the ratio of the Franck–Condon factors $\sigma_0^1/0_0^0$ is small (about 1/60), indicating that no other bands in this progression should be observable, and suggesting that there is virtually no change in the equilibrium position of the AT–Ar van der Waals bond length upon electronic excitation.

2. AT–Ar_2 symmetric stretch

The small peak at 18 397 cm^{-1}, about 41 cm^{-1} to the blue of the AT–Ar_2 origin, increases as the square of the argon concentration. Backing pressure studies show that this peak is not a hot band; this transition is thus a $+41$ cm^{-1} low frequency vibration of AT–Ar_2. In general, a rare gas atom bound to an aromatic ring exerts an exceedingly

weak perturbation on the electronic structure of the ring; thus, the potential experienced by each of the argon atoms in a di-argon complex must be virtually identical to that experience by the single argon atom in the binary complex. Weber[25] has pointed out that when the above condition is true, the frequency of the symmetric stretch of a complex of two rare gas atoms bound to opposite faces of an aromatic ring is related to the frequency of the symmetric stretch of the binary complex by, what in our system becomes

$$\omega_{\text{AT-AR}_2} = [M_{\text{AT}}/(M_{\text{AT}} + M_{\text{AT-Ar}})]^{1/2}\omega_{\text{AT-Ar}}, \quad (1)$$

where $\omega_{\text{AT-Ar}}$ and $\omega_{\text{AT-Ar}_2}$ are the frequencies of the symmetric stretch for AT–Ar and AT–Ar_2, and M_{AT} and $M_{\text{AT-Ar}}$ are the masses of the AT monomer and the binary complex, respectively. Using our previously assigned value of 44 cm^{-1} for the AT–Ar symmetric stretch, this relationship predicts σ_0^1 for AT–Ar_2 to be 37.3 cm^{-1}, which agrees moderately well with our observed + 41 cm^{-1} vibration. We thus assign this transition at 18 397 cm^{-1} as σ_0^1 of AT–Ar_2, which results in a wave number of 41 cm^{-1} for the symmetric stretch. This σ_0^1 transition is down in intensity by about a factor of 30 from the intensity of the AT–Ar_2 origin. This small Franck–Condon factor for σ_0^1 implies that there is very little change in the van der Waals bond lengths upon electronic excitation.

There is an exceedingly weak transition at 18 436 cm^{-1}, which argon concentration studies reveal to be a vibration of the AT–Ar_2 complex. This shift of + 81 cm^{-1} with respect to the AT–Ar_2 origin places this transition in the region expected for σ_0^2, and we thus assign this feature as the first overtone of the symmetric stretch. The drop in intensity of σ_0^2 relative to σ_0^1 is about a factor of 3, much smaller than the 30-fold decrease going from the origin to σ_0^1. If this assignment is correct, the position of σ_0^2 implies little anharmonicity at this level of the van der Waals potential.

3. The AT–Ar_2 isomer

The peak at 18 374 cm^{-1} increases quadratically with argon concentration, and thus is a transition associated with AT–Ar_2. This feature is located + 18 cm^{-1} from the AT–Ar_2 origin. At first glance, this appears to be an excellent candidate for a van der Waals bending vibration. However two problems arise from this assignment. First, this peak is one sixth the size of the AT–Ar_2 origin. Such a large intensity for a van der Waals bending transition implies a significant shift in equilibrium geometry along the van der Waals bending coordinate upon electronic excitation. A large geometry change upon electronic excitation is not supported by high resolution rotationally resolved spectra discussed in Sec. V, nor has such a large geometry change between ground and excited states ever been observed in similar van der Waals complexes. Secondly, if this feature is indeed the bending β_0^1 transition (β_0^2 if the mode is non-totally symmetric), then its large Franck–Condon factors imply that β_0^2 (β_0^4 if the mode is non-totally symmetric) would be sufficiently intense as to be easily observable with our experimental sensitivity. We see no feature at + 36 cm^{-1} (2×18 cm^{-1}) from the AT–Ar_2 origin. Thus, this interpretation is problematic.

We have an alternate explanation for this assignment. This feature is shifted 9 cm^{-1} to the red of the AT–Ar origin. This shift is the same as the band shift of AT–Ar_3 relative to AT–Ar_2. The third argon atom of AT–Ar_3, in analogy with T–Ar_3, is believed to bind to an argon atom already bound to the ring. Thus, perhaps this feature is the origin transition of an isomer of AT–Ar_2 where both argon atoms are bound to the same side of the ring. The first atom binds in the usual position, and the second atom lies above this previously bound argon. Thus, both argons would lie on the same side of the ring. High resolution spectroscopy would definitively answer this question; however, spectral congestion from overlapping peaks prevent us from resolving rotational structure in this transition. Thus, this assignment must remain tentative.

IV. SINGLE VIBRONIC LEVEL DISPERSED FLUORESCENCE SPECTRA

A. Excite AT–Ar origin

Figure 3 shows the emission spectrum obtained by exciting the AT–Ar origin at 18 383 cm^{-1}, taken at a resolution of 8.7 cm^{-1}. This spectrum is virtually identical to the single vibronic level (SVL) spectrum of the monomer origin, with a uniform band shift of all fluorescence bands by 27 cm^{-1} to the red, in agreement with the band shift in the excitation spectrum. All bands in the spectrum, with four exceptions, are found in the SVL spectrum of the parent molecule origin, and can be assigned in terms of known ring vibrations. The frequency of all the vibrational modes used to assign the transitions are identical to those of the AT monomer,[26] except for ν_{16b}, where $16b_2^0$ has a larger wave number of 257 cm^{-1} compared to 248 cm^{-1} in the parent molecule. Thus,

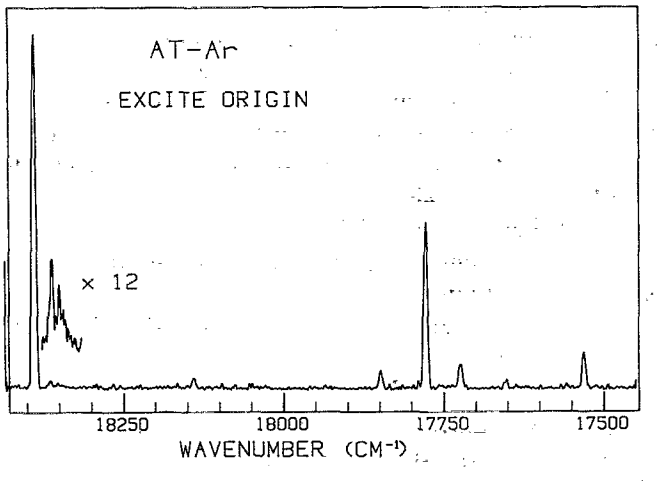

FIG. 3. The SVL dispersed emission spectrum obtained exciting the AT–Ar origin. The resolution is 8.7 cm^{-1}. About 5% of the intensity of the resonance band is due to scattered laser light.

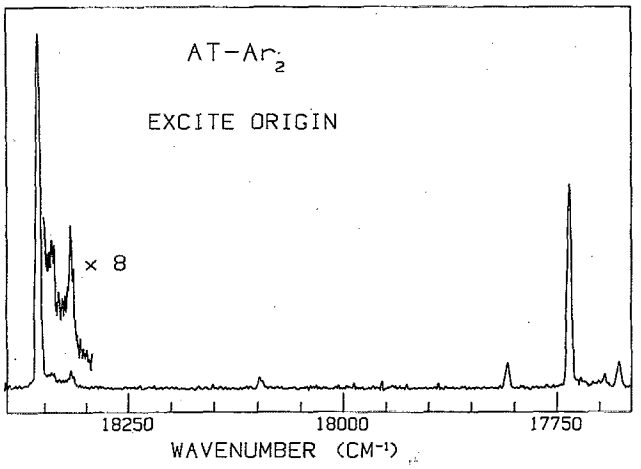

FIG. 4. The SVL dispersed emission spectrum obtained exciting the AT–Ar_2 origin. The resolution is 7.4 cm^{-1}. About 10% of the intensity of the resonance band is due to scattered laser light.

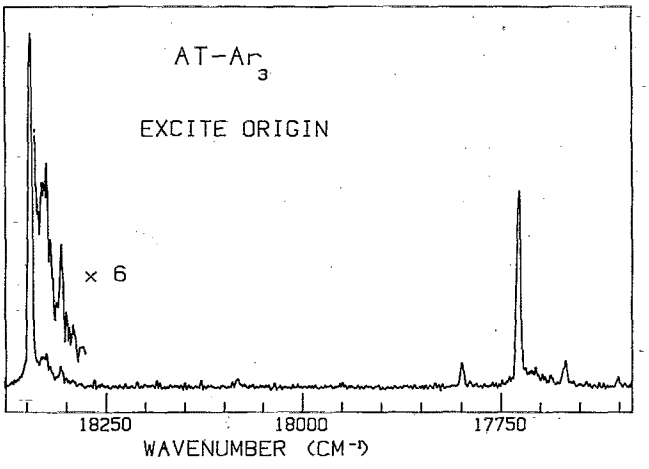

FIG. 5. The SVL dispersed emission spectrum obtained exciting the AT–Ar_3 origin. The resolution is 6.7 cm^{-1}. About 20% of the intensity of the resonance band is due to scattered laser light.

as in the excited state, the behavior of υ_{16b} is unique in AT in that it is the only mode we know of in which the frequency of the mode in the binary complex ($\upsilon'_{16b} = 223\ cm^{-1}$ and $\upsilon''_{16b} = 129\ cm^{-1}$) differs significantly from that of the monomer ($\upsilon'_{16b} = 215\ cm^{-1}$ and $\upsilon''_{16b} = 124\ cm^{-1}$).

The four features not assignable in terms of monomer ring vibrations are clearly due to low frequency van der Waals vibrations. These vibrations have a wave number of 25 and 42 cm^{-1}; they can each be seen in their fundamental transition near the origin, and in combination with $6a_1^0$. The 42 cm^{-1} vibration closely matches the 42.1 cm^{-1} wave number of the ground state van der Waals stretching vibration of T–Ar,[25] and thus we assign the feature at $-42\ cm^{-1}$ as σ_1^0. The σ_1^0 transition is reduced in intensity by about a factor of 80 relative to the origin, which is consistent with both the low resolution excitation scans, and the rotationally resolved spectra (*vide infra*) in indicating that there is little geometry change in the van der Waals bond length upon electronic excitation. The $-25\ cm^{-1}$ vibration is most likely one of the two van der Waals bends. The β_y bending mode (see Fig. 1) is non-totally symmetric in the molecular symmetry group of the complex, and hence only even overtones are allowed, while the β_z mode is totally symmetric, and all of its transitions are allowed. Thus, the $-25\ cm^{-1}$ feature can be attributed to either β_{z1}^0 or β_{y2}^0. We prefer the second assignment, as it implies $\upsilon_{\beta y} = 13\ cm^{-1}$, similar to the value of 15.5 cm^{-1} for this mode in the T–Ar ground state[25]; however no definitive statements can be made based on this data.

B. Excite AT–Ar_2 origin

Figure 4 shows the SVL spectrum obtained upon excitation of the origin transition of AT–Ar_2, taken at a resolution of 7.4 cm^{-1}. Once again, all but four of the features are assignable as transitions involving known ring vibrations. As in the binary complex, the frequency of all the ring modes are identical to those of the parent molecule with the exception of υ_{16b}, in which $\upsilon''_{16b} = 131\ cm^{-1}$. The four features not assignable in terms of ring modes are the fundamentals and $6a_1$ combination bands of -15 and $-38\ cm^{-1}$ van der Waals vibrations. We assign the $-38\ cm^{-1}$ vibration as the fundamental of the van der Waals symmetric stretch. This is in reasonable agreement with the value of $-36\ cm^{-1}$ predicted using Eq. 1, based on the $-42\ cm^{-1}$ wave number for σ_1^0 of AT–Ar. The intensity of σ_1^0 for AT–Ar_2 is reduced 20-fold relative to the 0_0^0 transition, indicating little geometry change upon electronic excitation, in agreement with low resolution excitation spectra and the rotationally resolved studies. The feature at $-15\ cm^{-1}$ is likely due to either a fundamental or first overtone (depending if the mode is totally symmetric or non-totally symmetric) of one of the four van der Waals bending modes.

C. Excite AT–Ar_3 origin

Figure 5 exhibits the dispersed emission spectrum of the AT–Ar_3 origin transition, taken at a resolution of about 6.7 cm^{-1}. There are now nine van der Waals vibrational modes, and classifying them as stretches, bends, or more complicated motions must await a normal coordinate analysis. We see two van der Waals vibrations, both by themselves, and in combination with υ_{6a}, having wavenumbers of -17 and $-39\ cm^{-1}$. The full width at half maximum of the $-17\ cm^{-1}$ feature is wider than our instrumental resolution; thus, it most likely contains several overlapping transitions. These overlapping transitions, being very low in frequency, most likely involve vibrational normal modes which have large bending components to their motions, as their frequencies are similar to the bending frequencies of AT–Ar and AT–Ar_2. Likewise, the higher frequency feature at $-39\ cm^{-1}$ is likely due to a normal mode whose motion contains a large stretching component.

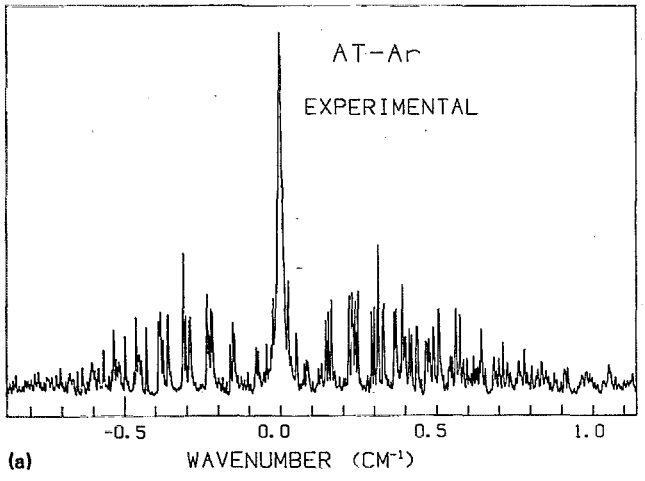

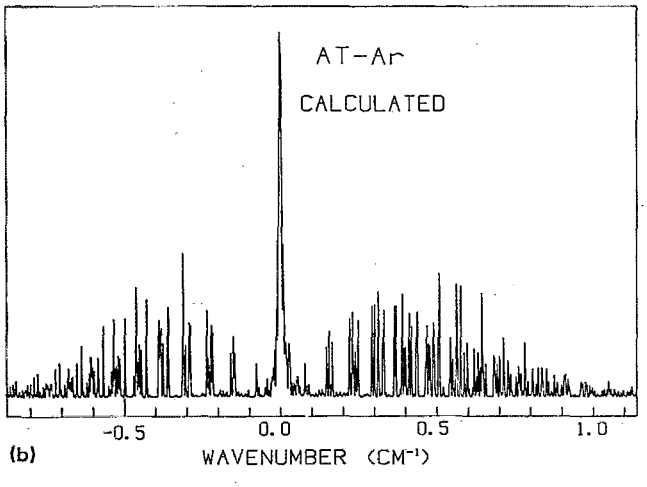

FIG. 6. (a) High resolution rotationally resolved spectrum of the AT–Ar origin, taken at a resolution of about 100 MHz. With the exception of the central Q branch, almost all of the lines are single rovibronic transitions. (b) Calculated rotational spectrum of AT–Ar, generated using the molecular parameters in the text.

V. ROTATIONALLY RESOLVED (HIGH RESOLUTION) FLUORESCENCE EXCITATION SPECTRA

A. AT–Ar

Figure 6(a) shows a high resolution rotationally resolved spectrum of the 0_0^0 band of AT–Ar taken using a single frequency ring dye laser. The spectrum has a resolution of about 100 MHz, caused primarily by Doppler broadening. The lifetime of the AT origin is 154 ns,[16] and the nominal linewidth of the ring laser is 0.5 MHz, so both these factors have a negligible effect on our spectral resolution. A resolution of 100 MHz is sufficiently high so that, with the exception of the intense Q-branch, the great majority of the spectral features in Fig. 6(a) are single rovibronic transitions, and congestion caused by overlapping transitions is not a problem.

Our method of fitting the spectrum has been described previously,[27] and only a brief description will be given here. We make an initial guess of the various molecular parameters, such as transition moment direction, rotational constants in the ground and excited states, and rotational temperature, and calculate the corresponding rotational spectrum. From this initial calculated spectrum, we can often assign the transitions for a number of lines in the experimental spectrum. These assigned rotational transitions were then fit to the observed molecular frequencies, varying the molecular parameters to give the best fit. All together a total of 111 lines were fit. Frequency assignments for these lines are available in Table I in supplementary material from PAPS.[27] As we were only fitting the line positions, we only varied the rotational constants in the ground and excited states. The transition moment direction and rotational temperature affect only the line intensities, not line positions; these parameters were varied manually to give the best match to the experimental spectrum. A single rotational temperature failed to give a good match to the experimental spectrum. This is not surprising, as a single temperature implies an equilibrium distribution, and the clusters formed in a supersonic jet are far from equilibrium. We consequently used the following two-temperature model to match the ground state rotational population:

$$P_i = \exp(-E_i/kT_1) + W\exp(-E_i/kT_2), \qquad (2)$$

where P_i is the population of the ith rotational level at energy E_i, T_1, and T_2 are the two rotational temperatures, and W is a factor which weights the relative contribution of T_1 and T_2. Manually varying T_1, T_2, and W in our calculated spectrum yielded good agreement with the experimental spectrum when $T_1 = 2.0$ K, $T_2 = 5.0$ K, and $W = 0.11$. The transition moment is out of the plane of the tetrazine ring,[26] as this is an $n \rightarrow \pi^*$ transition. Projection onto the inertial axis yields a transition moment which in the ground state is 94.4% A type and 5.6% C type, and in the excited state is 93.4% A type and 6.6% C type, as shown in Table III. The nuclear spin statistics for the AT–Ar complex are 17, 19, 17, and 19 for the *ee*, *eo*, *oe*, and *oo* rotational levels, respectively. Figure 6(b) shows a calculated spectrum generated using the above molecular parameters.

Our best fit rotational parameters are shown in Table III. The B and C rotational constants are determined to a much higher precision than the A rotational constant. The asymmetry parameter κ is -0.575 and -0.511 in the ground and excited states, respectively, indicating that AT–Ar is a moderately asymmetric top. In the limit as κ approaches -1, the molecule becomes a prolate symmetric top with a parallel polarized transition. Thus, for $\kappa = -1$, the experimental uncertainty in the A rotational constant approaches infinity, since the corresponding symmetric top spectrum is completely insensitive to the A rotational constant. Evidently AT–Ar is near enough to the symmetric top limit to have an order of magnitude more uncertainty in A'

TABLE III. Rotational constants and transition moment direction of AT–Ar derived from fitting the rotationally resolved fluorescence excitation spectrum of the origin band.

Parameter		Ground state	Excited state
Rotational constants (cm^{-1})	A	$0.069\,05 \pm 0.000\,31$	$0.068\,70 \pm 0.000\,31$
	B	$0.041\,923 \pm 0.000\,025$	$0.042\,891 \pm 0.000\,022$
	C	$0.034\,603 \pm 0.000\,018$	$0.034\,532 \pm 0.000\,017$
Asymmetry parameter[a]	κ	-0.5750	-0.5108
Transition moment direction[b]	A	0.9715	0.9662
	B	0.0000	0.0000
	C	-0.2370	-0.2578

[a] Dimensionless parameter.
[b] Projection of the transition moments upon the inertial axes of the AT–Ar complex.

TABLE IV. Geometric parameters of the AT–Ar complex deduced from the rotational constants in Table III.

Parameters[a]		Ground state	Excited state
Fit 1 (in Å)	x	3.335 ± 0.009	3.303 ± 0.009
	y	0.00 (fixed)	0.00 (fixed)
	z	0.01 ± 0.05	0.00 ± 0.04
Fit 2 (in Å)	x	3.346 ± 0.009	3.314 ± 0.008
	y	0.00 (fixed)	0.00 (fixed)
	z	0.73 ± 0.05	0.75 ± 0.04

[a] Parameters are the coordinates of the argon atom, as described in the text.

and A'' than in the other rotational constants. As we will see later, this problem becomes even more acute in AT–Ar_2.

From the rotational constants obtained from our fit, we can extract geometrical information regarding the AT–Ar complex. The AT–Ar complex has 27 vibrational degrees of freedom; obviously a complete structure determination is impossible. We decided to simplify this problem by noting that the argon atom is only an exceedingly weak perturbation on the parent molecule, and the structure of the AT subunit in AT–Ar is almost certainly virtually identical to the geometry of the bare AT monomer. Thus, we decided to fix the AT chromophore at the geometry we had previously determined for the monomer,[26] and vary only the position of the argon atom. This reduced the vibrational degrees of freedom to three, which we chose as the x, y, and z coordinates of the argon atom, with the center of the coordinate system at the center of the tetrazine ring, and the axes defined as in Fig. 1. AT has a plane of symmetry along the x–z plane; thus, the argon atom is likely to have a y coordinate of zero, except in the unlikely event of a double minima van der Waals potential. We thus fixed the y coordinate of the argon atom at zero, and varied the x and z coordinates. As there are three constraints on the system in each electronic state (the three rotational constants), we are able to solve this problem by fitting the x and z coordinates to match the experimentally determined rotational constants.

Table IV shows the results of our fit. Two sets of parameters match the rotational constants equally well. In the first fit the argon is centered over the ring ($y = z = 0$), while the other fit has the argon displaced toward the amino nitrogen by 0.73 and 0.78 Å in the ground and excited states, respectively. In Table V we have calculated the rotational constants obtained by setting the AT subunit in its ground state geometry, fixing the y coordinate of the argon at zero and the x coordinate at 3.32 Å, and varying the z coordinate. Starting at $z = 0$, the rotational constants begin changing in a given direction until, at about $z = 0.40$ Å, the change reverses directions and begins to reproduce rotational constants for smaller values of z. Thus, except for the value of $z = 0.40$ Å, where the argon atom is directly over the center of mass of the ring, there are always two values of z that will generate almost exactly the same rotational constants. This can be explained by considering the inertial axes of the AT–Ar cluster. The A inertial axis essentially is on the line connecting the argon atom to the center of mass of the AT subunit. Figure 7 shows the structure of the two possible geometries of AT–Ar from the fit, drawn so that their respective A inertial axes are parallel. These structures essentially differ only in the angle α which the plane of the ring makes with the B inertial axis. This angle α changes in sign but has the same magnitude in both structures. As the moment of inertia depends on the distance of the various atoms from the inertial axes, which in turn depends only on the absolute value of α, both structures have the same rotational constants, and would yield identical rotational spectra. This problem did not arise in the previously studied T–Ar complex, as the argon atom was located over the center of the ring which, by the symmetry of the molecule, was also the center of mass of the tetrazine chromophore. This is the one point above the ring where the rotational constants generated are unique; if the argon atom is displaced from over the center of the ring, then an equal displacement in the opposite

TABLE V. Rotational constants of AT–Ar calculated as a function of the z coordinate of the argon atom.

z coordinate[a] (Å)	Rotational constants (cm^{-1})		
	A	B	C
0.00	0.069 035	0.042 030	0.034 916
0.10	0.068 494	0.042 457	0.035 068
0.20	0.068 110	0.042 773	0.035 181
0.30	0.067 893	0.042 964	0.035 252
0.40	0.067 854	0.043 024	0.035 282
0.50	0.067 995	0.042 950	0.035 270
0.60	0.068 311	0.042 746	0.035 217
0.70	0.068 793	0.042 421	0.035 122
0.80	0.069 428	0.041 988	0.034 980
0.90	0.070 201	0.041 461	0.034 811

[a] The y and x coordinates are fixed at 0.00 and 3.32 Å, respectively.

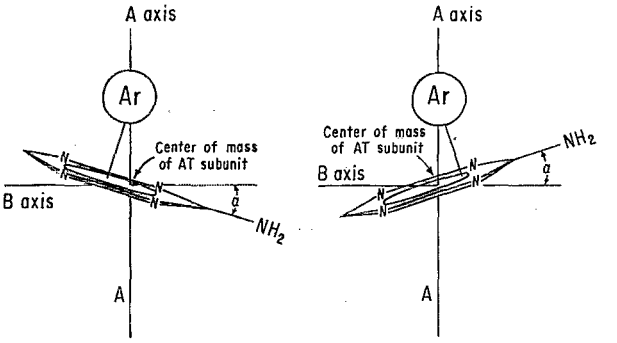

FIG. 7. The two possible geometries of AT–Ar. The A inertial axis runs from the argon atom through the center of mass of the AT subunit. Both structures have the same rotational constants.

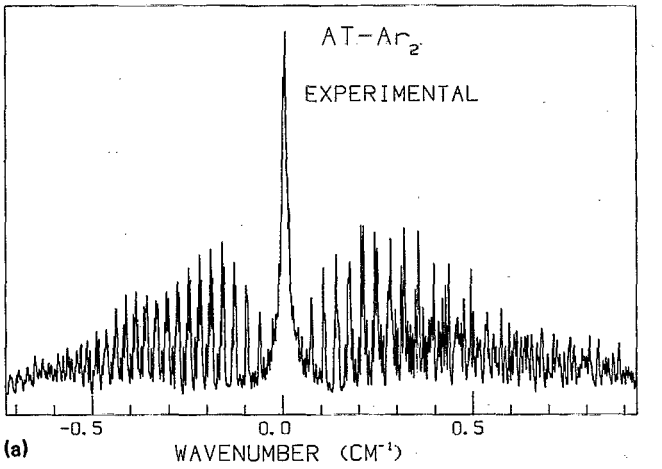

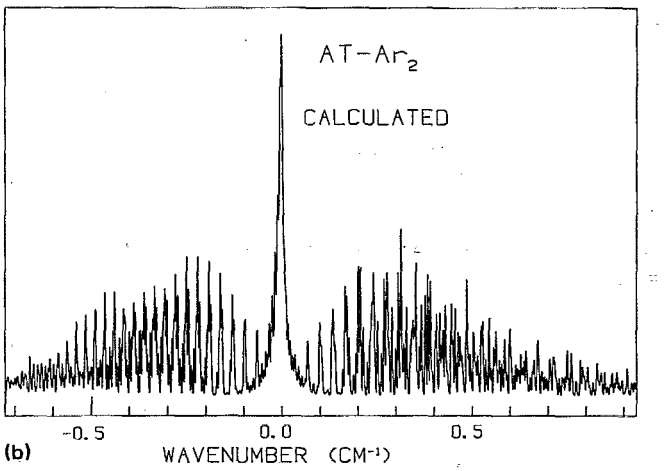

FIG. 8. (a) High resolution rotationally resolved spectrum of the AT–Ar_2 origin, taken at a resolution of about 90 MHz. (b) Calculated rotational spectrum of AT–Ar_2, generated using the molecular parameters described in the text.

direction will generate another structure with identical moments of inertia. In AT–Ar, the argon is definitely not over the center of mass of the AT monomer ($z = 0.41$ Å), so there are two structures, displaced by equal amounts but in opposite directions from the center of mass ($z = 0.01 \pm 0.05$ and 0.73 ± 0.05 Å in the ground state, and $z = 0.00 \pm 0.05$ and 0.75 ± 0.05 Å in the excited state) which match our experimentally determined rotational constants equally well.

In all previously studied systems in which a rare gas atom is bound to a single ring aromatic molecule, the rare gas atom was found to be bound to the center of the ring. This structure turns up as one of the fits in both the ground and excited state of AT–Ar. Thus, we believe fit 1 to be the correct fit, although fit 2 cannot be conclusively excluded based on our experimental evidence. Thus, it appears that even a strongly perturbative substituent, such as an amino group which is conjugated into the π system of the ring, is not strong enough to deform the electronic structure of the ring sufficiently to displace the argon from the center. Thus, while the amino group undoubtedly causes changes in the charge density at various points of the ring, to a large extent the electronic structure and charge distribution of the ring must resemble that of the tetrazine molecule.

The argon atom is located 3.335 ± 0.009 Å from the ring plane in the ground state; upon electronic excitation the separation changes only very slightly, decreasing to 3.303 ± 0.009 Å. The very small magnitude of this change in the van der Waals bond length is consistent with the very weak $\Delta v = 1$ transitions for the AT–Ar van der Waals stretching vibration in both excitation and emission. This van der Waals bond length is about 0.1 Å shorter than that of T–Ar[15] (ground state, 3.429 ± 0.006 Å; excited state, 3.40 ± 0.01 Å) which suggests that perhaps the argon is bound more strongly in AT–Ar than in T–Ar. This observation, however, does not seem to be supported by our studies on the binding energy of the AT–Ar complex.[16]

B. AT–Ar_2

Figure 8(a) shows the high resolution rotationally resolved spectrum of the origin transition of AT–Ar_2, taken at a resolution of about 90 MHz. The rotational constants of AT–Ar_2 are sufficiently small so that overlapping transitions are becoming a problem, and a significant minority of the features in Fig. 6 are not single rovibronic transitions. We nonetheless are able to find sufficient numbers of single rovibronic transitions to be able to use peak positions and assignments to fit the rotational constants. Altogether 93 line positions were fit. Frequency assignments are available in Table II in supplementary material submitted to PAPS.[27] The rotational constants generated are shown in Table VI. The ground state rotational population was well matched by setting $T_1 = 2.2$ K, $T_2 = 7.0$ K, and $W = 0.15$. The transition is polarized out of the plane of the tetrazine ring; when projected onto the inertial axes it becomes virtually a pure A type transition. As the symmetry of AT–Ar_2 is the same as that of AT, and the argon atoms have a nuclear spin of zero,

TABLE VI. Rotational constants and transition moment direction of AT–Ar_2 derived from fitting the rotationally resolved fluorescence excitation spectrum of the origin band.

Parameter		Ground state	Excited state
Rotational constants (cm $^{-1}$)	A	0.067 3 ± 0.004 8	0.066 7 ± 0.004 8
	B	0.017 083 ± 0.000 031	0.017 443 ± 0.000 032
	C	0.015 607 ± 0.000 031	0.015 674 ± 0.000 034
Asymmetry parameter[a]	κ	− 0.942 9	− 0.934 1
Transition moment direction[b]	A	0.999 99	0.999 99
	B	− 0.003 18	− 0.003 82
	C	0.000 00	0.000 00

[a] Dimensionless parameter.
[b] Projection of the transition moments upon the inertial axes of the AT–Ar_2 complex.

the nuclear spin statistics for AT–Ar_2 are the same as for AT, namely 17, 17, 19, and 19 for the *ee*, *eo*, *oe*, and *oo* rotational levels, respectively. Figure 8(b) shows a calculated spectrum generated using the above values of the molecular parameters.

Upon inspection of the experimental spectrum in Fig. 7(a), it becomes clear that AT–Ar_2 is a near symmetric top molecule with a parallel polarized transition (i.e., the transition moment is parallel to the unique inertial axis). This is reflected in the experimentally determined asymmetry parameter κ of − 0.9429 and − 0.9341 in the ground and excited states, respectively (see Table VI), very close to the value of − 1.0 for a perfect prolate symmetric top. As the spectrum of a prolate symmetric top is completely insensitive to the value of the A rotational constant, one would expect an experimental fit to a near prolate symmetric top to yield values for A' and A'' with large experimental uncertainties. This is reflected in Table VI, where the uncertainties in the A rotational constants are two orders of magnitude larger than those for the B and C rotational constants. Our experimental resolution was just high enough to enable us to use the K splittings to extract an approximate value for A' and A''.

We can use these rotational constants to obtain geometrical information about the AT–Ar_2 complex. Once again, we fix the AT subunit at the geometry determined for the ground and excited states of the AT monomer, which reduces the number of vibrational degrees of freedom from 30 to six. We choose these six parameters to be the x, y, and z coordinates of each of the two argon atoms. As before, we make use of the symmetry of the molecule to fix the value of the y coordinate of both argon atoms as zero, since it is very unlikely that the van der Waals potential surface is a double minimum potential. Finally, we require the z coordinate of both atoms to be equal, and the x coordinates to be equal in magnitude and opposite in sign. This forces both argon atoms to be bound to equivalent sites on opposite sides of the tetrazine ring, which we known to be the case as the origin transitions of AT–Ar and AT–Ar_2 obey the band shift rule. This leaves us with two parameters. As the rotational constants impose three constraints on the system, it is possible to find a solution. Table VII gives the results of our fits. The large error bars, particularly on the y parameter, are caused by the uncertainty in the A rotational constants, and reflect the intrinsically lesser amount of information obtainable from a parallel polarized near symmetric top transition. Once again there are two sets of parameters which match the rotational constants equally well. If we fix the value of y and x and calculate the rotational constants for a range of z values, we see similar behavior to what occurs for the AT–Ar complex as was shown in Table V. Except for the value of $z = 0.40$ Å, where the argon atoms are centered above and below the center of mass of the tetrazine ring, there will always be two values of z that will generate the same rotational constants. This is a general problem that will appear in these types of systems whenever the argon atoms do not lie directly above and below the center of mass of the parent

TABLE VII. Geometric parameters of the AT–Ar_2 complex deduced from the rotational constants in Table VI.

Parameters[a]		Ground state	Excited state
Fit 1 (in Å)	x	3.369 ± 0.014	3.337 ± 0.015
	y	0.00 (fixed)	0.00 (fixed)
	z	0.1 ± 0.6	0.1 ± 0.6
Fit 2 (in Å)	x	3.369 ± 0.014	3.337 ± 0.015
	y	0.00 (fixed)	0.00 (fixed)
	z	0.7 ± 0.6	0.8 ± 0.6

[a] Parameters are the coordinates of the argon atoms, with the y and z coordinate of both argon atoms being equal, and the x coordinate of the second argon equal to minus that of the first argon, as described in the text.

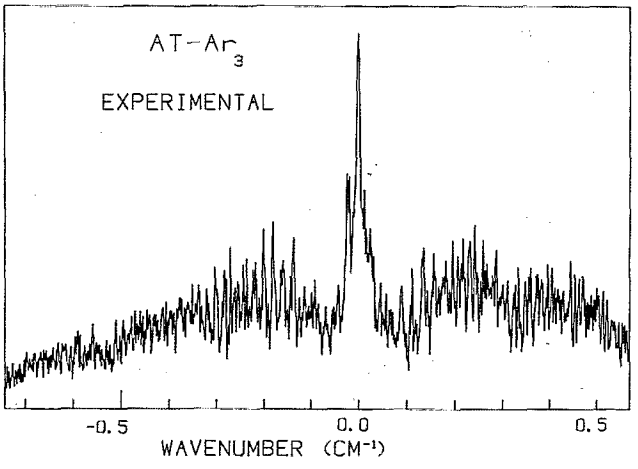

FIG. 9. High resolution spectrum of the AT–Ar_3 origin, taken at a resolution of about 90 MHz. The extreme spectral congestion and multiple Q branches indicate spectral contamination from other argon–AT cluster species.

molecule. Despite the large error bars of the fits in Table VII, it is apparent that one fit places the argon atom approximately over the center of the ring, while the other fit puts the atoms on the opposite side of the center of mass of the AT subunit, at about $z = 0.7$ Å. For reasons stated in the previous section, we believe fit 1 to be the correct fit, with the argon atom sitting over the center of the ring. Once again, it appears that the amino group is not a sufficiently strong perturbation on the electronic structure of the tetrazine ring to displace the argon atoms from the center of the ring.

The length of the van der Waals bond is almost the same in the two electronic states, decreasing only slightly upon electronic excitation (ground, 3.369 ± 0.014 Å; excited, 3.337 ± 0.015 Å). This van der Waals bond length is about 0.1 Å shorter than the corresponding bond length in T–Ar_2 (ground, 3.424 ± 0.005 Å; excited 3.421 ± 0.005 Å), which suggests that the argon atoms in AT–Ar_2 are bound more tightly than in T–Ar_2. This conclusion, however, does not seem to be supported by binding energy studies.[16]

C. AT–Ar_3

The high resolution spectrum of the origin transition of AT–Ar_3 can be seen in Fig. 9. The spectrum is exceedingly congested; each feature in the system is likely due to many overlapping transitions. Part of this can be attributed to the smaller rotational constants resulting from the larger moments on inertia of AT–Ar_3. These smaller rotational constants, however, cannot fully account for the extreme congestion in Fig. 9, and some other factor must be contributing. Looking at the low resolution fluorescence excitation spectrum in Fig. 2(d), we see that the AT–Ar_3 origin is located upon the center of a broad hill, in a region with many spectral transition. The broad features in this region are due to higher oligomer of AT with argon, which can exist in a variety of isomers. Thus, the extreme congestion we see in the high resolution spectrum of AT–Ar_3 reflects contamination from other complexes of argon and AT. This is supported by the multiple Q-branch transitions seen in Fig. 9, which suggest transitions are occurring from multiple cluster species. As we are unable to mass select our species of interest, we have no way of eliminating this contamination, and thus are unable to do the complete rotational analysis of the AT–Ar_3 origin. About all that can be said is that the sharp central Q branch is consistent with a structure having the third argon atom lying above an argon already bound to the ring, but many other structures are also consistent with this observation.

ACKNOWLEDGMENTS

This work was supported by the National Science Foundation under Grant No. CHE-8818321. J.C.A. gratefully acknowledges support under the National Science Foundation Graduate Fellowship Program. S.J.M. acknowledges support under the Illinois Minority Graduate Fellowship Program. We are indebted to Dr. D. D. Yang for synthesis of the sample of aminotetrazine.

[1] R. E. Smalley, L. Wharton, D. H. Levy, and D. W. Chandler, J. Chem. Phys. **68**, 2487 (1978).
[2] D. V. Brumbaugh, J. E. Kenny, and D. H. Levy, J. Chem. Phys. **78**, 3415 (1982).
[3] J. J. F. Ramaekers, H. K. van Dijk, J. Langelaar, and R. R. H. Rettschnick, Faraday Discuss. Chem. Soc. **75**, 183 (1983).
[4] J. J. F. Ramaekers, L. B. Krignen, H. J. Lips, J. Langelaar, and R. P. H. Raeeschnick, Laser Chem. **2**, 125 (1983).
[5] M. Heppener, A. G. M. Kunst, D. Bebelaar, and R. P. H. Rettschnick, J. Chem. Phys. **83**, 5341 (1985).
[6] P. Weber and S. A. Rice, J. Chem. Phys. **88**, 6120 (1989).
[7] T. A. Stephenson and S. A. Rice, J. Chem. Phys. **81**, 1083 (1984).
[8] K. Yamanouchi, S. Isogai, S. Tsuchiya, and K. Kuchitsu, Chem. Phys. **116**, 123 (1987).
[9] C. A. Haynam, D. V. Brumbaugh, and D. H. Levy, J. Chem. Phys. **81**, 2282 (1984).
[10] H. Abe, Y. Ohyanagi, M. Ichijo, N. Mihami, and M. Ito, J. Phys. Chem. **89**, 3512 (1985).
[11] B. A. Jacobson, S. Humphrey, and S. A. Rice, J. Chem. Phys. **89**, 5624 (1988).
[12] H.-K. O, C. S. Parmenter, and M. C. Su, Ber. Bunsenges, Phys. Chem. **92**, 253 (1988).
[13] O. Dimopoulou-Rademann, U. Even, A. Amirav, and J. Jortner, J. Phys. Chem. **92**, 5371 (1988).
[14] E. J. Bieske, M. W. Rainbird, I. M. Atkinson, and A. E. Knight, J. Chem. Phys. **91**, 752 (1989).
[15] C. A. Haynam, D. V. Brumbaugh, and D. H. Levy, J. Chem. Phys. **80**, 2253 (1983).
[16] J. C. Alfano, S. J. Martinez, and D. H. Levy, J. Chem. Phys. **91**, 7302 (1989).
[17] D. Osborn, J. C. Alfano, and D. H. Levy (unpublished results).
[18] R. E. Smalley, L. Wharton, and D. H. Levy, J. Mol. Spectrosc. **66**, 375 (1977).
[19] D. V. Brumbaugh, C. A. Haynam, and D. H. Levy, J. Mol. Spectrosc. **94**, 316 (1982).
[20] R. E. Smalley, D. H. Levy, and L. Wharton, J. Chem. Phys. **64**, 3266 (1976).
[21] H. H. Takimoto and C. C. Denault, Tetrahedron Lett. **44**, 5369 (1966).
[22] A. D. Counotte-Potman and H. C. vanderPlass, J. Heterocyclic Chem. **15**, 445 (1987).
[23] W. Sharfin, K. E. Johnson, L. Wharton, and D. H. Levy, J. Chem. Phys. **71**, 1292 (1979).
[24] J. A. Menapace and E. R. Bernstein, J. Phys. Chem. **91**, 2533 (1987).
[25] P. M. Weber, J. T. Buontempo, F. Novak, and S. A. Rice, J. Chem. Phys. **88**, 6082 (1988).
[26] J. C. Alfano, S. J. Martinez, and D. H. Levy, J. Mol. Spectrosc. **143**, 366 (1990).
[27] See AIP document number PAPS JCPSA-94-1673-9 for 9 pages of supplementary material Tables I and II. Order by PAPS number and journal reference from American Institute of Physics, Physics Auxiliary Publication Service, 335 East 45th St., New York, NY 10017. The price is $1.50 for each microfiche (98 pages) or $5.00 for photocopies of up to 30 pages, and $0.15 for each additional page over 30 pages. Airmail additional. Make checks payable to the American Institute of Physics.